Simulation of flow in fractured poroelastic media: a comparison of different discretization approaches

I. Ambartsumyan[1], E. Khattatov[1], I. Yotov[1], and P. Zunino[2]

[1] Department of Mathematics, University of Pittsburgh, Pittsburgh, PA 15260, ILA6@pitt.edu, ELK58@pitt.edu, yotov@math.pitt.edu

[2] Department of Mechanical Engineering & Materials Science, University of Pittsburgh, Pittsburgh, PA 15261, paz13@pitt.edu

Abstract. We study two finite element computational models for solving coupled problems involving flow in a fracture and flow in poroelastic media. The Brinkman equation is used in the fracture, while the Biot system of poroelasticity is employed in the surrounding media. Appropriate equilibrium and kinematic conditions are imposed on the interfaces. We focus on the approximation of the interface conditions, which in this context feature the interaction of different variables, such as velocities, displacements, stresses and pressures. The aim of this study is to compare the Lagrange multiplier and the Nitsche's methods applied to enforce these non standard interface conditions.

1 Problem set up

We consider a multiphysics model problem for flow in fractured and deformable porous media, where the simulation domain $\Omega \subset \mathbf{R}^d$, $d = 2, 3$, is a union of non-overlapping and possibly non-connected regions Ω_f and Ω_p. Here Ω_f is a fluid region with flow governed by the Brinkman equations and Ω_p is a poroelasticity region governed by the Biot system for coupled Darcy and elasticity equations. Let $\Gamma_{fp} = \partial\Omega_f \cap \partial\Omega_p$. Let $(\mathbf{u}_\star, p_\star)$ be the velocity-pressure pairs in $\Omega_\star$, $\star = f$, p, and let $\boldsymbol{\eta}_p$ be the displacement in Ω_p. Let ν be the fluid viscosity, K the symmetric and uniformly positive definite rock permeability tensor, $\mathbf{f}_\star$ body force terms, and $q_\star$ external source or sink terms. Let $\mathbf{D}(\mathbf{u}_f)$ and $\boldsymbol{\sigma}_f(\mathbf{u}_f, p_f)$ denote, respectively, the deformation rate tensor and the stress tensor:

$$\mathbf{D}(\mathbf{u}_f) = \frac{1}{2}(\nabla\mathbf{u}_f + \nabla\mathbf{u}_f^T), \quad \boldsymbol{\sigma}_f(\mathbf{u}_f, p_f) = -p_f\mathbf{I} + 2\nu\mathbf{D}(\mathbf{u}_f).$$

In the fracture region Ω_f, $(\mathbf{u}_f, p_f)$ satisfy the Brinkman equations

$$-\nabla\cdot\boldsymbol{\sigma}_f(\mathbf{u}_f, p_f) + \nu K_f^{-1}\mathbf{u}_f = \mathbf{f}_f, \qquad \nabla\cdot\mathbf{u}_f = q_f \quad \text{in } \Omega_f, \tag{1}$$

where K_f represents the fracture permeability. Let $\boldsymbol{\sigma}_e(\boldsymbol{\eta})$ and $\boldsymbol{\sigma}_p(\boldsymbol{\eta}, p)$ be the elasticity and poroelasticity stress tensor, respectively:

$$\boldsymbol{\sigma}_e(\boldsymbol{\eta}) = \lambda_p(\nabla\cdot\boldsymbol{\eta})\mathbf{I} + 2\mu_p\mathbf{D}(\boldsymbol{\eta}), \quad \boldsymbol{\sigma}_p(\boldsymbol{\eta}, p) = \boldsymbol{\sigma}_e(\boldsymbol{\eta}) - \alpha p\mathbf{I}, \tag{2}$$

where α is the Biot-Willis constant. The poroelasticity region Ω_p is governed by the quasi-static Biot system [3]

$$-\nabla \cdot \boldsymbol{\sigma}_p(\boldsymbol{\eta}_p, p_p) = \mathbf{f}_p \quad \text{in } \Omega_p, \tag{3}$$

$$\nu K^{-1}\mathbf{u}_p + \nabla p_p = 0, \qquad \frac{\partial}{\partial t}(s_0 p_p + \alpha \nabla \cdot \boldsymbol{\eta}_p) + \nabla \cdot \mathbf{u}_p = q_p \quad \text{in } \Omega_p, \tag{4}$$

where s_0 is a storage coefficient. The *interface conditions* on the fluid-poroelasticity interface Γ_{fp} are *mass conservation*, *balance of normal stress*, and the Beavers-Joseph-Saffman (BJS) law [2, 13] modeling *slip with friction* [14, 1]:

$$\mathbf{u}_f \cdot \mathbf{n}_f + (\frac{\partial \boldsymbol{\eta}_p}{\partial t} + \mathbf{u}_p) \cdot \mathbf{n}_p = 0, \tag{5}$$

$$-(\boldsymbol{\sigma}_f \mathbf{n}_f) \cdot \mathbf{n}_f = p_p, \tag{6}$$

$$-(\boldsymbol{\sigma}_f \mathbf{n}_f) \cdot \boldsymbol{\tau}_{f,j} = \nu \alpha_{BJS} \sqrt{K_j^{-1}} (\mathbf{u}_f - \frac{\partial \boldsymbol{\eta}_p}{\partial t}) \cdot \boldsymbol{\tau}_{f,j} \quad \text{on } \Gamma_{fp}, \tag{7}$$

as well as *conservation of momentum*:

$$(\boldsymbol{\sigma}_f \mathbf{n}_f) \cdot \mathbf{n}_f = (\boldsymbol{\sigma}_p \mathbf{n}_p) \cdot \mathbf{n}_p, \quad (\boldsymbol{\sigma}_f \mathbf{n}_f) \cdot \boldsymbol{\tau}_{f,j} = (\boldsymbol{\sigma}_p \mathbf{n}_p) \cdot \boldsymbol{\tau}_{p,j} \quad \text{on } \Gamma_{fp}, \tag{8}$$

where $\mathbf{n}_f$ and $\mathbf{n}_p$ are the outward unit normal vectors to $\partial\Omega_f$, and $\partial\Omega_p$, respectively, $\boldsymbol{\tau}_{f,j}$, $1 \le j \le d-1$, is an orthogonal system of unit tangent vectors on Γ_{fp}, $K_j = (K\boldsymbol{\tau}_{f,j}) \cdot \boldsymbol{\tau}_{f,j}$, and $\alpha_{BJS} > 0$ is an experimentally determined friction coefficient. We note that the continuity of flux takes into account the normal velocity of the solid skeleton, while the BJS condition accounts for its tangential velocity.

2 Numerical approximation

Our discretization approach is based on the finite element method. For this reason, we consider the weak formulation of the Biot-Brinkman system (1), (3)–(4). It is obtained by multiplying the equations in each region by suitable test functions, integrating by parts certain terms, and utilizing the interface and boundary conditions. For simplicity the latter are assumed to be homogeneous: $\mathbf{u}_f = 0$, $\mathbf{u}_p \cdot \mathbf{n}_p = 0$ and $\boldsymbol{\eta}_p = 0$ on $\partial\Omega$. Let $(\cdot,\cdot)_S$, $S \subset \mathbf{R}^d$, be the $L^2(S)$ inner product and let $\langle \cdot, \cdot \rangle_F$, $F \subset \mathbf{R}^{d-1}$, be the $L^2(F)$ inner product or duality pairing. Let us define

$$\begin{aligned}
&\mathbf{V}_f = H^1(\Omega_f)^d, \quad W_f = L^2(\Omega_f),\\
&\mathbf{V}_p = H(\mathrm{div}; \Omega_p), \quad W_p = L^2(\Omega_p),\\
&\mathbf{X}_p = H^1(\Omega_p)^d.
\end{aligned}$$

The global spaces are products of the subdomain spaces and satisfy the boundary conditions. For simplicity assume for the moment that each region consists of a

single subdomain. Let $b_\star(\mathbf{v}, w) = -(\nabla \cdot \mathbf{v}, w)_{\Omega_\star}$ and let

$$\begin{aligned} a_f(\mathbf{u}_f, \mathbf{v}_f) &= (2\nu \mathbf{D}(\mathbf{u}_f) : \mathbf{D}(\mathbf{v}_f)_{\Omega_f} + (\nu K_f^{-1} \mathbf{u}_f, \mathbf{v}_f), \\ a_p^d(\mathbf{u}_p, \mathbf{v}_p) &= (\nu K^{-1} \mathbf{u}_p, \mathbf{v}_p)_{\Omega_p}, \\ a_p^e(\boldsymbol{\eta}_p, \boldsymbol{\xi}_p) &= (\boldsymbol{\sigma}_e(\boldsymbol{\eta}_p) : \mathbf{D}(\boldsymbol{\xi}_p))_{\Omega_p}. \end{aligned}$$

be the bilinear forms related to Brinkman, Darcy and the elasticity operators, respectively.

To proceed with the discretization, we denote with $\mathbf{V}_{f,h}, W_{f,h}$ the finite element spaces for the velocity and pressure approximation on the fluid domain Ω_f, with $\mathbf{V}_{p,h}, W_{p,h}$ the spaces for velocity and pressure approximation on the porous matrix Ω_p and with $\mathbf{X}_{p,h}$ the approximation spaces for the structure displacement. We assume that all the finite element approximation spaces comply with the prescribed Dirichlet conditions on external boundaries $\partial\Omega_f$, $\partial\Omega_p$. For the time discretization, we denote with t_n the current time step and with d_τ the first order (backward) discrete time derivative $d_\tau u^n := \tau^{-1}(u^n - u^{n-1})$.

2.1 Approximation of interface conditions using the Lagrange multiplier method

To impose the interface conditions on Γ_{fp} we introduce a Lagrange multiplier $\lambda_h \in \Lambda_h = (\mathbf{V}_{p,h} \cdot \mathbf{n}_p)'$ with a physical meaning $\lambda_h = -(\boldsymbol{\sigma}_{f,h}\mathbf{n}_f) \cdot \mathbf{n}_f$. Then, we seek $\mathbf{u}_{f,h} \in \mathbf{V}_{f,h}$, $p_{f,h} \in W_{f,h}$, $\mathbf{u}_{p,h} \in \mathbf{V}_{p,h}$, $p_{p,h} \in W_{p,h}$, $\boldsymbol{\eta}_{p,h} \in \mathbf{X}_{p,h}$, and $\lambda_h \in \Lambda_h$ such that for all $\mathbf{v}_{f,h} \in \mathbf{V}_{f,h}$, $w_{f,h} \in W_{f,h}$, $\mathbf{v}_{p,h} \in \mathbf{V}_{p,h}$, $w_{p,h} \in W_{p,h}$, $\boldsymbol{\xi}_{p,h} \in \mathbf{X}_{p,h}$, and $\mu_h \in \Lambda_h$,

$$\begin{aligned} a_f(\mathbf{u}_{f,h}, \mathbf{v}_{f,h}) + a_p^d(\mathbf{u}_{p,h}, \mathbf{v}_{p,h}) + a_p^e(\boldsymbol{\eta}_{p,h}, \boldsymbol{\xi}_{p,h}) + a_{BJS}(\mathbf{u}_{f,h}, \boldsymbol{\eta}_{p,h}; \mathbf{v}_{f,h}, \boldsymbol{\xi}_{p,h}) \\ + b_f(\mathbf{v}_{f,h}, p_{f,h}) + b_p(\mathbf{v}_{p,h}, p_{p,h}) + \alpha b_p(\boldsymbol{\xi}_{p,h}, p_{p,h}) + b_\Gamma(\mathbf{v}_{f,h}, \mathbf{v}_{p,h}, \boldsymbol{\xi}_{p,h}; \lambda_h) \\ = (\mathbf{f}_{f,h}, \mathbf{v}_{f,h})_{\Omega_f} + (\mathbf{f}_{p,h}, \boldsymbol{\xi}_{p,h})_{\Omega_p}, \quad (9) \end{aligned}$$

$$\begin{aligned} (s_0 d_\tau p_{p,h}, w_{p,h}) - \alpha b_p(d_\tau \boldsymbol{\eta}_{p,h}, w_{p,h}) - b_p(\mathbf{u}_{p,h}, w_{p,h}) - b_f(\mathbf{u}_{f,h}, w_{f,h}) \\ = (q_{f,h}, w_{f,h})_{\Omega_f} + (q_{p,h}, w_{p,h})_{\Omega_p}, \quad (10) \end{aligned}$$

$$b_\Gamma(\mathbf{u}_{f,h}, \mathbf{u}_{p,h}, d_\tau \boldsymbol{\eta}_{p,h}; \mu_h) = 0, \quad (11)$$

where

$$a_{BJS}(\mathbf{u}_f, \boldsymbol{\eta}_p; \mathbf{v}_f, \boldsymbol{\xi}_p) = \sum_{j=1}^{d-1} \langle \nu \alpha_{BJS} \sqrt{K_j^{-1}} (\mathbf{u}_f - \frac{\partial \boldsymbol{\eta}_p}{\partial t}) \cdot \boldsymbol{\tau}_{f,j}, (\mathbf{v}_f - \boldsymbol{\xi}_p) \cdot \boldsymbol{\tau}_{f,j} \rangle_{\Gamma_{fp}},$$

$$b_\Gamma(\mathbf{v}_f, \mathbf{v}_p, \boldsymbol{\xi}_p; \mu) = \langle \mathbf{v}_f \cdot \mathbf{n}_f + (\boldsymbol{\xi} + \mathbf{v}_p) \cdot \mathbf{n}_p, \mu \rangle_{\Gamma_{fp}}.$$

We note that the balance of normal stress, BJS, and conservation of momentum interface conditions (7)–(8) are natural and have been utilized in the derivation of

the weak formulation, while the conservation of mass condition in (7) is imposed weakly in (11).

We solve problem (9)-(10)-(11) using piecewise linear finite elements for the approximation of all the variables. It is well known that the equal-order approximation is unstable for saddle point problems such as Darcy, Stokes or Brinkman [4]. For this reason, we complement the discretization of Brinkman problem, namely (1), with the Brezzi-Pitkaranta stabilization operator acting on the pressure [5, 4]. Owing to the pressure time derivative in equation (4) the Biot system is not a saddle point problem. For this reason, pressure stabilization is not required. Particular attention should be also devoted to the discretization of the Lagrange multiplier space. For the piecewise linear approximation adopted here, we observe that the Lagrange multiplier space coincides with the normal components of the interface trace spaces of $\mathbf{V}_{f,h}$, $\mathbf{V}_{p,h}$, $\mathbf{X}_{p,h}$. This property has two important consequences. First, it is straightforward to show that equation (11) is exactly satisfied. Second, owing to the results obtained in [12] for general elliptic problems and the more recent analysis of Stokes-Darcy equations [9], it can be shown that this property entails the unique solvability of the discrete system.

Besides the well posedness of the finite element method, stability of the time discretization must be also addressed. To this purpose, by taking

$$(\mathbf{v}_{f,h}, w_{f,h}, \mathbf{v}_{p,h}, w_{p,h}, \boldsymbol{\xi}_{p,h}, \mu) = (\mathbf{u}^n_{f,h}, p^n_{f,h}, \mathbf{u}^n_{p,h}, p^n_{p,h}, d_\tau \boldsymbol{\eta}^n_{p,h}, \lambda_h)$$

in (9)–(11) we obtain an energy equality

$$\begin{aligned} &a_f(\mathbf{u}^n_{f,h}, \mathbf{u}^n_{f,h}) + a^d_p(\mathbf{u}^n_{p,h}, \mathbf{u}^n_{p,h}) + a^e_p(\boldsymbol{\eta}^n_{p,h}, d_\tau \boldsymbol{\eta}^n_{p,h}) \\ &+\sum_{j=1}^{d-1} \nu \alpha_{BJS} \|K_j^{-1/4}(\mathbf{u}^n_{f,h} - d_\tau \boldsymbol{\eta}^n_{p,h}) \cdot \boldsymbol{\tau}_{f,j}\|^2_{L^2(\Gamma_{fp})} + (d_\tau s_0 p^n_{p,h}, p^n_{p,h}) = \mathcal{F}(t_n; \mathbf{u}_{f,h}) \end{aligned}$$

Using the following equality

$$\int_\Omega u^n d_\tau u^n = \frac{1}{2} d_\tau \|u^n\|^2_\Omega + \frac{1}{2}\tau \|d_\tau u^n\|^2_\Omega$$

the energy equality becomes

$$\begin{aligned} &\frac{1}{2} d_\tau \left(s_0 \|p^n_{p,h}\|^2_{L^2(\Omega_p)} + a^e_p(\boldsymbol{\eta}^n_{p,h}, \boldsymbol{\eta}^n_{p,h}) \right) + \frac{\tau}{2} \left(s_0 \|d_\tau p^n_{p,h}\|^2_{L^2(\Omega_p)} + a^e_p(d_\tau \boldsymbol{\eta}^n_{p,h}, d_\tau \boldsymbol{\eta}^n_{p,h} \right) \\ &+ a_f(\mathbf{u}^n_{f,h}, \mathbf{u}^n_{f,h}) + a^d_p(\mathbf{u}^n_{p,h}, \mathbf{u}^n_{p,h}) + \sum_{j=1}^{d-1} \nu \alpha_{BJS} \|K_j^{-1/4}(\mathbf{u}^n_{f,h} - d_\tau \boldsymbol{\eta}^n_{p,h}) \cdot \boldsymbol{\tau}_{f,j}\|^2_{L^2(\Gamma_{fp})} = \mathcal{F}(t_n; \mathbf{u}_{f,h}) \end{aligned}$$

Rearranging the following terms,

$$\begin{aligned} a_f(\mathbf{u}^n_{f,h}, \mathbf{u}^n_{f,h}) + a^d_p(\mathbf{u}^n_{p,h}, \mathbf{u}^n_{p,h}) + \frac{\tau}{2} a^e_p(d_\tau \boldsymbol{\eta}^n_{p,h}, d_\tau \boldsymbol{\eta}^n_{p,h}) \\ = 2\nu \|\mathbf{D}(\mathbf{u}^n_{f,h})\|^2_{\Omega_f} + \nu K^{-1} \|\mathbf{u}^n_{p,h}\|^2_{\Omega_p} + \frac{\tau}{2} \|d_\tau \nabla \cdot \boldsymbol{\eta}^n_{p,h}\|_{\Omega_p} \end{aligned}$$

using the bound on generic forcing term,

$$\mathcal{F}(t_n;\mathbf{u}^n_{f,h}) \leq (2\epsilon'\nu)^{-1}\|\mathcal{F}(t_n)\|^2 + \frac{\epsilon'}{2}\nu\|\mathbf{D}(\mathbf{u}^n_{f,h})\|^2_{\Omega_f},$$

and combining these results and summing up with respect to time index $n = 1, ..., N$, the following energy estimate is obtained.

Theorem 1. *For any $\epsilon' > 0$, the discrete problem* (9)-(10)-(11) *satisfies the following energy estimate:*

$$\begin{aligned}
&\frac{1}{2}\left(s_0\|p^n_{p,h}\|^2_{L^2(\Omega_p)} + a^e_p(\boldsymbol{\eta}^n_{p,h},\boldsymbol{\eta}^n_{p,h})\right)\\
&\quad + \tau\sum_{n=1}^{N}\Big[2\nu(1-\frac{\epsilon'}{4})\|\mathbf{D}(\mathbf{u}_{f,h})\|^2_{\Omega_f} + \nu K_f^{-1}\|\mathbf{u}_{f,h}\|^2_{\Omega_f} + \nu K^{-1}\|\mathbf{u}_{p,h}\|^2_{\Omega_p}\\
&+\frac{\tau}{2}\left(\|d_\tau\nabla\cdot\boldsymbol{\eta}^n_{p,h}\|_{\Omega_p} + s_0\|d_\tau p^n_{p,h}\|\right) + \sum_{j=1}^{d-1}\nu\alpha_{BJS}\|K_j^{-1/4}(\mathbf{u}_{f,h} - \frac{\partial\boldsymbol{\eta}_{p,h}}{\partial t})\cdot\boldsymbol{\tau}_{f,j}\|^2_{L^2(\Gamma_{fp})}\Big]\\
&\qquad \leq \frac{1}{2}\left(s_0\|p^0_{p,h}\|^2_{L^2(\Omega_p)} + a^e_p(\boldsymbol{\eta}^0_{p,h},\boldsymbol{\eta}^0_{p,h})\right) + \tau\sum_{n=1}^{N}(2\epsilon'\nu)^{-1}\|\mathcal{F}(t_n)\|^2. \quad (12)
\end{aligned}$$

2.2 Approximation of interface conditions by Nitsche's method

The enforcement of interface conditions by means of Lagrange multipliers leads to an accurate but expensive problem at the discrete level. For this reason, some alternatives have been developed. The most straightforward strategy consists in the application of a penalty method. The idea is to enrich the variational formulation with new terms corresponding to additional quadratic functionals which are minimized when the Dirichlet boundary conditions are exactly satisfied. The penalty method, however, suffers from lack of consistency with respect to the continuous formulation of the problem. Among several interpretations, Nitsches method can be seen as a variant of the penalty method. Indeed, it allows to weakly enforce boundary and interface conditions and it restores the strong consistency of the discrete scheme with respect to the continuous form of the variational formulation. For an introduction to this technique applied to general boundary and interface conditions we refer to [10], while this method is applied to FSI in [7], and to the Biot-Stokes system in [6].

Applying Nitsche's method to equations (1), (3)–(4) with the corresponding interface and boundary conditions, we obtain the following discrete problem formulation, that consists of a system of three coupled problems: for any index $n > 0$, find $\boldsymbol{\eta}^n_h \in \mathbf{X}_{p,h}$, $\boldsymbol{u}^n_{p,h} \in \mathbf{V}_{p,h}$, $p^n_{p,h} \in W_{p,h}$ and $\boldsymbol{u}^n_{f,h} \in \mathbf{V}_{f,h}$, $p^n_{f,h} \in W_{f,h}$ such that for any $\forall\boldsymbol{\xi}_h \in \mathbf{X}_{p,h}$, $\boldsymbol{v}_{p,h} \in \mathbf{V}_{p,h}$, $w_{p,h} \in W_{p,h}$, $\boldsymbol{v}_{f,h} \in \mathbf{V}_{f,h}$, $w_{f,h} \in W_{f,h}$ the following equations are satisfied:

$$
\begin{aligned}
&a_p^e(\boldsymbol{\eta}_h^n, \boldsymbol{\xi}_h) - b_p(p_{p,h}^n, \boldsymbol{\xi}_h) + \langle \boldsymbol{n}_p \cdot \boldsymbol{\sigma}_{f,h} \boldsymbol{n}_p \, , \big(- \boldsymbol{\xi}_h \big) \cdot \boldsymbol{n}_p \rangle_{\Gamma_{fp}} \qquad (13)\\
&+ \langle \nu \alpha_{BJS} \sqrt{K_j^{-1}} d_\tau \boldsymbol{\eta}_h^n \cdot \boldsymbol{t}_p \, , \boldsymbol{\xi}_h \cdot \boldsymbol{t}_p \rangle_{\Gamma_{fp}} \; + \langle \gamma \nu h^{-1} d_\tau \boldsymbol{\eta}_h^n \cdot \boldsymbol{n}_p \, , \boldsymbol{\xi}_h \cdot \boldsymbol{n}_p \rangle_{\Gamma_{fp}} \\
&- \langle \nu \alpha_{BJS} \sqrt{K_j^{-1}} \boldsymbol{u}_{f,h}^n \cdot \boldsymbol{t}_p \, , \boldsymbol{\xi}_h \cdot \boldsymbol{t}_p \rangle_{\Gamma_{fp}} - \langle \gamma \nu h^{-1} \big(\boldsymbol{u}_{f,h}^n - \boldsymbol{u}_{p,h}^n \big) \cdot \boldsymbol{n}_p \, , \boldsymbol{\xi}_h \cdot \boldsymbol{n}_p \rangle_{\Gamma_{fp}} = 0,
\end{aligned}
$$

$$
\begin{aligned}
&s_0(d_\tau p_{p,h}^n \, , w_{p,h})_{\Omega_p} + a_p(\boldsymbol{u}_{p,h}^n, \boldsymbol{v}_{p,h}) - b_p(p_{p,h}^n, \boldsymbol{v}_{p,h}) + b_p(w_{p,h}, \boldsymbol{u}_{p,h}^n) \qquad (14)\\
&+ \langle \gamma \nu h^{-1} \boldsymbol{u}_{p,h}^n \cdot \boldsymbol{n}_p \, , \boldsymbol{v}_{p,h} \cdot \boldsymbol{n}_p \rangle_{\Gamma_{fp}} + b_s(w_{p,h}, d_\tau \boldsymbol{\eta}_h^n) \\
&- \langle \gamma \nu h^{-1} \big(\boldsymbol{u}_{f,h}^n - d_\tau \boldsymbol{\eta}_h^n \big) \cdot \boldsymbol{n}_p \, , \boldsymbol{v}_{p,h} \cdot \boldsymbol{n}_p \rangle_{\Gamma_{fp}} - \langle \boldsymbol{n}_p \cdot \boldsymbol{\sigma}_{f,h} \boldsymbol{n}_p \, , \boldsymbol{v}_{p,h} \cdot \boldsymbol{n}_p \rangle_{\Gamma_{fp}} = 0,
\end{aligned}
$$

$$
\begin{aligned}
&\langle \rho_f d_\tau \boldsymbol{u}_{f,h}^n \, , \boldsymbol{v}_{f,h} \rangle_{\Omega_f} + a_f(\boldsymbol{u}_{f,h}^n, \boldsymbol{v}_{f,h}) - b_f(p_{f,h}^n, \boldsymbol{v}_{f,h}) + b_f(w_{f,h}, \boldsymbol{u}_{f,h}^n) \qquad (15)\\
&- \langle \boldsymbol{n}_f \cdot \boldsymbol{\sigma}_{f,h} \boldsymbol{n}_f \, , \boldsymbol{v}_{f,h} \cdot \boldsymbol{n}_f \rangle_{\Gamma_{fp}} - \langle \boldsymbol{n}_f \cdot \boldsymbol{\sigma}_{f,h} (\varsigma \boldsymbol{v}_{f,h}, -w_{f,h}) \boldsymbol{n}_f \, , \boldsymbol{u}_{f,h}^n \cdot \boldsymbol{n}_f \rangle_{\Gamma_{fp}} \\
&+ \langle \boldsymbol{n}_f \cdot \boldsymbol{\sigma}_{f,h} (\varsigma \boldsymbol{v}_{f,h}, -w_{f,h}) \boldsymbol{n}_f \, , \big(\boldsymbol{u}_{p,h}^n + d_\tau \boldsymbol{\eta}_h^n \big) \cdot \boldsymbol{n}_f \rangle_{\Gamma_{fp}} \\
&+ \langle \gamma \nu h^{-1} \boldsymbol{u}_{f,h}^n \cdot \boldsymbol{n}_f \, , \boldsymbol{v}_{f,h} \cdot \boldsymbol{n}_f \rangle_{\Gamma_{fp}} + \langle \nu \alpha_{BJS} \sqrt{K_j^{-1}} \boldsymbol{u}_{f,h}^n \cdot \boldsymbol{t}_f \, , \boldsymbol{v}_{f,h} \cdot \boldsymbol{t}_f \rangle_{\Gamma_{fp}} \\
&- \langle \gamma \nu h^{-1} \big(\boldsymbol{u}_{p,h}^n + d_\tau \boldsymbol{\eta}_h^n \big) \cdot \boldsymbol{n}_f \, , \boldsymbol{v}_{f,h} \cdot \boldsymbol{n}_f \rangle_{\Gamma_{fp}} - \langle \nu \alpha_{BJS} \sqrt{K_j^{-1}} d_\tau \boldsymbol{\eta}_h^n \cdot \boldsymbol{t}_f \, , \boldsymbol{v}_{f,h} \cdot \boldsymbol{t}_f \rangle_{\Gamma_{fp}} \\
&= \mathcal{F}(t^n; \boldsymbol{v}_{f,h}),
\end{aligned}
$$

where γ is a positive penalty (or stabilization) parameter and $\varsigma \in \{-1, 0, 1\}$ is a symmetry parameter that allows us to switch from the so called *symmetric, incomplete and skew-symmetric* problem formulations respectively. The value of γ will be determined below, in order to guarantee the stability of the scheme. To study the stability of the Nitsche's method, we use the following inverse inequality,

$$
h \| \boldsymbol{D}(\boldsymbol{u}_h) \boldsymbol{n} \|_{\Gamma_{fp}}^2 \leq C_{TI} \| \boldsymbol{D}(\boldsymbol{u}_h) \|_{\Omega_f}^2, \qquad (16)
$$

where C_{TI} is a positive constant uniformly upper bounded with respect to the mesh characteristic size h, for a family of shape-regular and quasi-uniform meshes [8]. Since we solve the FSI problem on fixed domains, the constant C_{TI} does not depend on the solution. The following result shows that the scheme (13)-(14)-(15) is stable for any time step.

Theorem 2. *[6] For any $\hat{\epsilon}', \check{\epsilon}'$ that satisfy*

$$
1 - \frac{(\varsigma + 1)}{2} \hat{\epsilon}' C_{TI} - \frac{\check{\epsilon}'}{2} > 0
$$

where $\varsigma \in \{-1, 0, 1\}$ provided that $\gamma > (\varsigma + 1)(\hat{\epsilon}')^{-1}$, there exist constants $0 < c < 1$ and $C > 1$, uniformly independent of the mesh characteristic size h, such

that

$$
\begin{aligned}
&\frac{1}{2}\Big(2\mu_p\|\boldsymbol{D}(\boldsymbol{\eta}_h^N)\|_{\Omega_p}^2+\lambda_p\|\nabla\cdot\boldsymbol{\eta}_h^N\|_{\Omega_p}^2+s_0\|p_{p,h}^N\|_{\Omega_p}^2\Big) \qquad (17)\\
&+c\tau\sum_{n=1}^{N}\Big[2\nu\|\boldsymbol{D}(\boldsymbol{u}_{f,h}^n)\|_{\Omega_f}^2+\nu K_f^{-1}\|\boldsymbol{u}_{f,h}^n\|_{\Omega_f}^2+\nu K^{-1}\|\boldsymbol{u}_{p,h}^n\|_{\Omega_p}^2\\
&+\frac{\tau}{2}\big(\rho_f\|d_\tau\boldsymbol{u}_{f,h}^n\|_{\Omega_f}^2+2\mu_p\|d_\tau\boldsymbol{D}(\boldsymbol{\eta}_h^n)\|_{\Omega_p}^2+s_0\|d_\tau p_{p,h}^n\|_{\Omega_p}^2+\lambda_p\|d_\tau\nabla\cdot\boldsymbol{\eta}_h^n\|_{\Omega_p}^2\big)\\
&+\nu h^{-1}\big(\|\big(\boldsymbol{u}_{f,h}^n-\boldsymbol{u}_{p,h}^n-d_\tau\boldsymbol{\eta}_h^n\big)\cdot\boldsymbol{n}\|_{\Gamma_{fp}}^2+\|\big(\boldsymbol{u}_{f,h}^n-d_\tau\boldsymbol{\eta}_h^n\big)\cdot\boldsymbol{t}\|_{\Gamma_{fp}}^2\big)\Big]\\
&\le\frac{1}{2}\Big(2\mu_p\|\boldsymbol{D}(\boldsymbol{\eta}_h^0)\|_{\Omega_p}^2+\lambda_p\|\nabla\cdot\boldsymbol{\eta}_h^0\|_{\Omega_p}^2+s_0\|p_{p,h}^0\|_{\Omega_p}^2\Big)\\
&+\tau\sum_{n=1}^{N}\frac{C}{\nu}\|\mathcal{F}(t_n)\|^2.
\end{aligned}
$$

More precisely, we have

$$
\begin{aligned}
&c<\min\{\big(1-\frac{(\varsigma+1)}{2}\hat{\epsilon}'C_{TI}-\frac{\check{\epsilon}'}{2}\big),\big((\gamma-(\varsigma+1)(\hat{\epsilon}')^{-1}\big)\},\\
&C>(2\check{\epsilon}')^{-1}.
\end{aligned}
$$

3 Computational results

We consider the test case motivated by the example investigated by Lesinigo et al in [11], Section 7.2. The computational domain consists of two unit squares separated by a fracture of width $\delta = 0.1$. The squares represent the poroelastic subdomains of Ω_p. We assume that there are no external forces or mass sources. On the left and right boundaries we impose the homogeneous Dirichlet pressure and the homogeneous Dirichlet displacement conditions, while on the remaining external boundaries we impose zero normal flux and zero normal poroelastic stress. In order to generate a nontrivial flow pattern, a uniform flow is enforced on the bottom side of the fracture $\mathbf{u}_f \cdot \boldsymbol{n} = 10$, while the upper side of Ω_f is impermeable to flow. We expect to observe a vertical flow in Ω_f, which progressively fades out moving upwards, because of a significant leakage of fluid into Ω_p. Since the friction term is active in the Brinkman equation, we also expect that the pressure decreases along the direction of the flow in Ω_f.

We first consider a test case (we refer to it as Case A) designed to verify the agreement with the example in [11]. Since there the tangential flow interface condition is free slip and the porous media is not deformable, we take $\alpha_{BJS} = 0$ and Young modulus $E_p = 10^{10}$ Pa (very hard material), see the parameter set in Table 1. Furthermore, we investigate the behavior of the model in a regime different from [11]. In particular, we choose $\alpha_{BJS} = 1$ (this configuration is called Case B) and finally we consider a softer material characterized by $E_p = 10^3$ Pa (this is denoted as Case C). All the problems were solved over the time interval $[0, 1]$ s with time step $\Delta t = 0.1s$.

Case A: $\alpha_{BJS} = 0$, $E_p = 10^{10}$ Pa

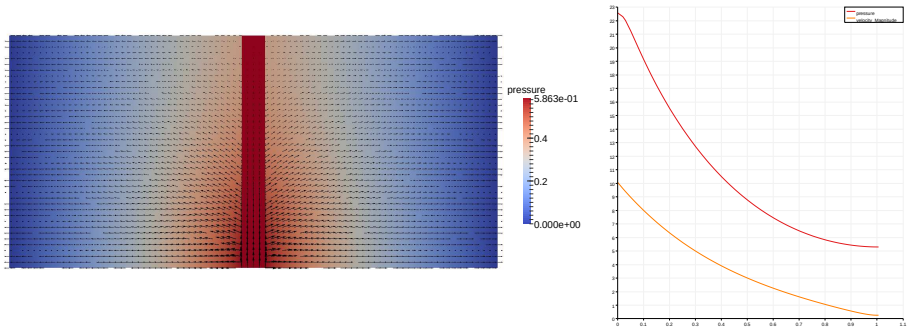

Case B: $\alpha_{BJS} = 1$, $E_p = 10^{10}$ Pa

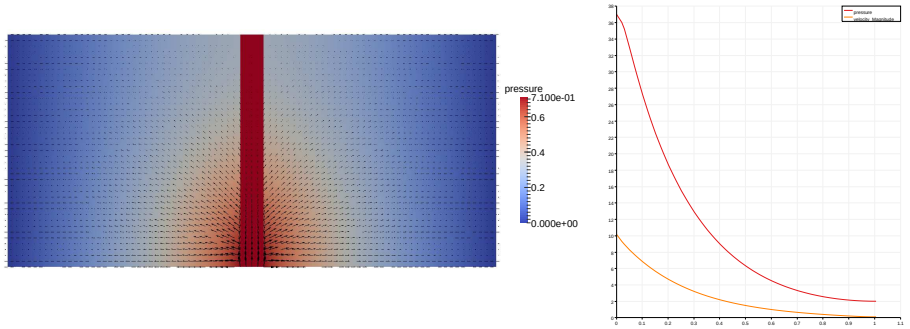

Case C: $\alpha_{BJS} = 1$, $E_p = 10^{3}$ Pa

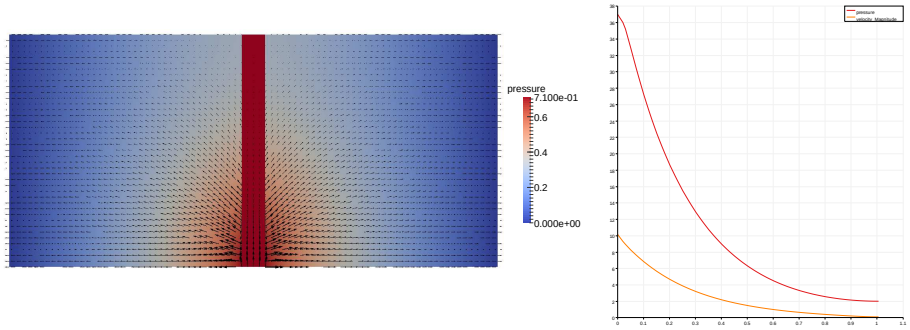

Fig. 1. Velocity glyphs at time $t = 1$. For visualization purposes, the velocity field on Ω_p has been magnified of a factor 10. The background color shows the pressure magnitude (left panel). Velocity and pressure plot along the vertical meanline of Ω_f (right panel).

Case A: $\alpha_{BJS} = 0$, $E_p = 10^{10}$ Pa

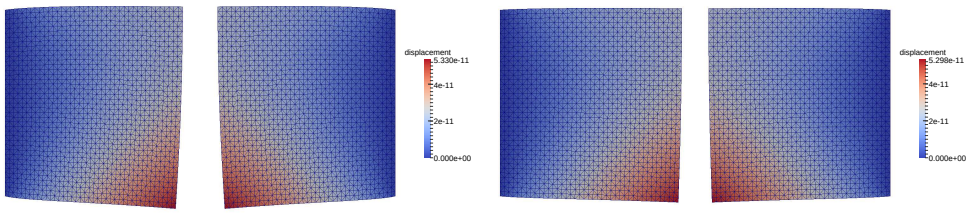

Case B: $\alpha_{BJS} = 1$, $E_p = 10^{10}$ Pa

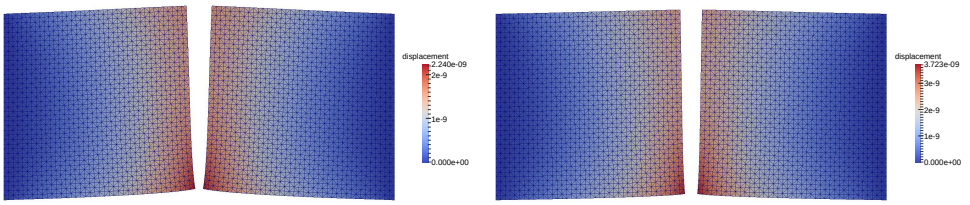

Case C: $\alpha_{BJS} = 1$, $E_p = 10^{3}$ Pa

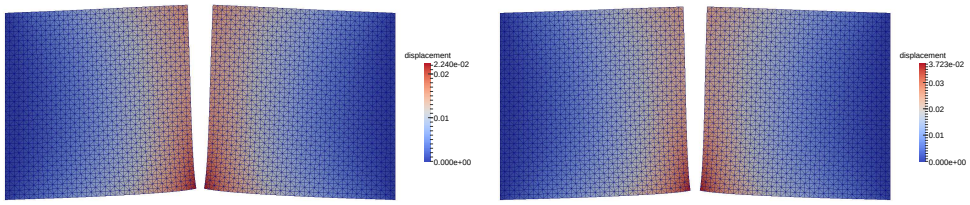

Fig. 2. Porous domain deformation at $t = 1$. The background color shows the fluid pressure magnitude. For visualization purposes, the displacement field has been magnified of a factor 10^7 for cases A and B. Results obtained with the Lagrange multiplier scheme are reported in the left, the ones corresponding to Nitsche's method are on the right.

Parameters	Values	Parameters	Values
Young modulus E_p (Pa)	10^{10}	**poisson ratio**	0.3
First Lamé param. μ_p(Pa)	$3.84\,10^9$	**Second Lamé param.** λ_p(Pa)	$5.76\,10^9$
Hydraulic conductivity νK^{-1}(m^3 s/Kg)	$\boldsymbol{I}$	**Mass storativity** s_0(Pa)	1
Biot-Willis constant α	1	**BJS friction coef.** α_{BJS}	0
Hydraulic conductivity K_f^{-1}(m^3 s/Kg)	$10\boldsymbol{I}$	**Brinkman viscosity** ν	1

Table 1. Poroelasticity and fluid parameters that are used in the numerical experiments denoted as Case A.

The simulation results obtained with the Lagrange multiplier method are reported in Figure 1. On the left we observe that the main expected features of the solution are correctly captured. For a more quantitative comparison, we plot on the right the variation of velocity modulus and pressure along the (vertical) meanline of Ω_f and we compare these results with the ones reported in Figure 7a of [11]. An excellent agreement is observed. The analysis of the problem configurations A, B, C shows that the BJS friction factor α_{BJS} significantly affects the pressure profile in the fluid region Ω_f. Because the friction has increased, but the flow rare is prescribed at the boundary, we observe a significant increase of the pressure at the inlet. The pressure field in the porous medium is also sensitive to this variation, but with less intensity. We finally notice that cases B and C look very similar. This suggests that the entire flow field is almost unaffected by the stiffness of the material.

The sensitivity of the model with respect to the interface BJS friction coefficient also emerges in Figure 2, where we show the displacement of the porous domain. In particular, we observe that the displacement field changes significantly when we move from $\alpha_{BJS} = 0$ to $\alpha_{BJS} = 1$. Furthermore, even though not revealed by the visualization because amplification factors are adopted, the displacement field is almost inversely proportional to the Young modulus of the solid material. We finally notice that, although $p_f > p_p$ along the fluid-solid interface, the fluid is inducing a traction on the solid in cases B and C. This effect happens in this specific problem configuration, because $p_f \simeq (2\nu\mathbf{D}(\mathbf{u}_f)\mathbf{n}_f)\cdot\mathbf{n}_f$ in Ω_f and as a result $(\boldsymbol{\sigma}_f(\mathbf{u}_f, p_f)\mathbf{n}_f)\cdot\mathbf{n}_f \simeq 0$. In the cases where $\alpha_{BJS} = 1$ the tangential interaction dominates over the normal one in the fluid-solid interaction. This justifies the differences between the displacement observed in cases A, B and C.

3.1 Comparison of Lagrange multiplier and Nitsche's methods

In this section we aim to accurately compare the two schemes proposed for the solution of the problem. First, from a preliminary inspection based on visualizations similar to the ones of Figures 1, we observe that the two methods provide very similar results. They also provide equivalent accuracy and precision as confirmed by the analysis of the convergence rate with respect to the mesh characteristic size, h, reported in Table 2. As error indicators, we consider the dominating terms that appear in the left hand sides of the stability estimates,

h	$\|e^N_{p,h}\|_{\Omega_p}$	rate	$\|\boldsymbol{D}(\mathbf{e}^N_{\eta,h})\|_{\Omega_p}$	rate	$\sqrt{\tau \sum_{n=1}^N \|\mathbf{e}^n_{\mathbf{u},f,h}\|^2_{\Omega_p}}$	rate	$\sqrt{\tau \sum_{n=1}^N \|\mathbf{e}^n_{\mathbf{u},p,h}\|^2_{\Omega_p}}$	rate
1/20	4.72E-02		4.03E-01		5.18E-02		1.77E-01	
1/40	1.35E-02	1.81	2.36E-01	0.77	1.94E-02	1.41	6.21E-02	1.51
1/80	3.38E-03	1.99	1.24E-01	0.93	5.97E-03	1.70	1.86E-02	1.74
1/160	6.93E-04	2.29	7.31E-02	0.76	1.40E-03	2.09	4.74E-03	1.98

h	$\|e^N_{p,h}\|_{\Omega_p}$	rate	$\|\boldsymbol{D}(\mathbf{e}^N_{\eta,h})\|_{\Omega_p}$	rate	$\sqrt{\tau \sum_{n=1}^N \|\mathbf{e}^n_{\mathbf{u},f,h}\|^2_{\Omega_p}}$	rate	$\sqrt{\tau \sum_{n=1}^N \|\mathbf{e}^n_{\mathbf{u},p,h}\|^2_{\Omega_p}}$	rate
1/20	8.68E-02		4.35E-01		1.24E-01		2.23E-01	
1/40	3.19E-02	1.44	2.56E-01	0.76	3.39E-02	1.87	9.08E-02	1.30
1/80	1.11E-02	1.52	1.35E-01	0.93	1.06E-02	1.67	2.85E-02	1.67
1/160	3.30E-03	1.75	8.02E-02	0.75	2.49E-03	2.10	7.51E-03	1.92

Table 2. Convergence analysis with respect to the mesh characteristic size for the Lagrange multiplier method (top) and Nitsche's method (bottom). Since an analytical solution is not available for the considered problem, we calculate the error with respect to a numerical solution computed on a highly refined mesh with $h = 1/320$ and denoted by $\widetilde{\mathbf{u}}_{f,h}\,, \widetilde{p}_{p,h}\,, \boldsymbol{D}(\widetilde{\boldsymbol{\eta}}_h)\,, \widetilde{\mathbf{u}}_{p,h}$. Then, the discretization error is given by $\mathbf{e}^N_{\mathbf{u},f,h} := \mathbf{u}^N_{f,h} - \widetilde{\mathbf{u}}^N_{f,h}\,, e^N_{p,h} := p^N_{p,h} - \widetilde{p}^N_{p,h}\,, \boldsymbol{D}(\mathbf{e}^N_{\eta,h}) := \boldsymbol{D}(\boldsymbol{\eta}^N_h) - \boldsymbol{D}(\widetilde{\boldsymbol{\eta}}^N_h)\,, \mathbf{e}^n_{\mathbf{u},p,h} := \mathbf{u}^n_{p,h} - \widetilde{\mathbf{u}}^n_{p,h}$. To facilitate the interpretation of the results, error norms are normalized with respect to the corresponding norm of the solution.

	Lagrange multipliers		Nitsche	
h	$\mathcal{R}_{\Gamma_1}$	$\mathcal{R}_{\Gamma_2}$	$\mathcal{R}_{\Gamma_1}$	$\mathcal{R}_{\Gamma_2}$
1/20	4.4402E-12	3.8642E-12	2.7522E-01	2.7528E-01
1/40	1.9694E-12	1.9698E-12	4.8690E-03	4.8690E-03
1/80	4.2337E-13	4.2424E-13	1.5374E-03	1.5374E-03
1/160	1.0735E-13	1.0568E-13	3.8450E-04	3.8450E-04
1/320	2.5801E-13	2.5472E-13	9.3927E-05	9.3927E-05

Table 3. The behavior of the indicator $\mathcal{R}_{\Gamma_i}(\mathbf{u}_{f,h}, \boldsymbol{\eta}_{p,h,}\mathbf{u}_{p,h})$ when varying the mesh characteristic size.

namely equations (12) and (17) for the Lagrange and Nitsche's methods respectively. Finally, since the main distinction between the two proposed methods consists of the enforcement of interface conditions, and in particular the mass conservation condition (5), we analyze in Table 3 the numerical residual

$$\mathcal{R}_{\Gamma_i}(\mathbf{u}_f, \boldsymbol{\eta}_p, \mathbf{u}_p) := \int_{\Gamma_i} \left(\mathbf{u}_f \cdot \mathbf{n}_f + (\frac{\partial \boldsymbol{\eta}_p}{\partial t} + \mathbf{u}_p) \cdot \mathbf{n}_p \right), \Gamma_i = \Omega_f \cap \Omega_{p,i}\,,\ i = 1, 2,$$

for the approximate solutions provided by each method. The results of Table 3 confirm the higher accuracy of the Lagrange multiplier method for the approximation of interface conditions. Indeed, Table 3 shows that the Lagrange multiplier method is exactly enforcing the desired condition at every interface

node. Conversely, equation (5) is only approximately enforced by the Nitsche's scheme and as expected the residual decreases proportionally with h.

Acknowledgments. The first three authors have been partially supported by the NSF grants DMS 1115856 and DMS 1418947. The third and fourth authors have been partially supported by the DOE grant DE-FG02-04ER25618. The authors thank Martina Bukac and Rana Zakerzadeh for their contribution to the development of the software used in this paper.

References

1. Badia, S., Quaini, A., Quarteroni, A.: Coupling Biot and Navier-Stokes equations for modelling fluid-poroelastic media interaction. J. Comput. Phys. 228(21), 7986–8014 (2009), http://dx.doi.org/10.1016/j.jcp.2009.07.019
2. Beavers, G., Joseph, D.: Boundary conditions at a naturally impermeable wall. J. Fluid. Mech 30, 197–207 (1967)
3. Biot, M.: General theory of three-dimensional consolidation. J. Appl. Phys. 12, 155–164 (1941)
4. Boffi, D., Brezzi, F., Fortin, M.: Mixed finite element methods and applications, Springer Series in Computational Mathematics, vol. 44. Springer, Heidelberg (2013), http://dx.doi.org/10.1007/978-3-642-36519-5
5. Brezzi, F., Pitkäranta, J.: On the stabilization of finite element approximations of the Stokes equations. In: Efficient solutions of elliptic systems (Kiel, 1984), Notes Numer. Fluid Mech., vol. 10, pp. 11–19. Friedr. Vieweg, Braunschweig (1984)
6. Bukac, M., Yotov, I., Zakerzadeh, R., Zunino, P.: Partitioning strategies for the interaction of a fluid with a poroelastic material based on a Nitsche's coupling approach. Comput. Methods Appl. Mech. Eng. (2014), http://dx.doi.org/10.1016/j.cma.2014.10.047
7. Burman, E., Fernández, M.A.: Stabilization of explicit coupling in fluid-structure interaction involving fluid incompressibility. Comput. Methods Appl. Mech. Eng. 198, 766–784 (2009)
8. Ern, A., Guermond, J.L.: Theory and practice of finite elements, Applied Mathematical Sciences, vol. 159. Springer-Verlag, New York (2004)
9. Girault, V., Vassilev, D., Yotov, I.: Mortar multiscale finite element methods for Stokes-Darcy flows. Numer. Math. 127(1), 93–165 (2014), http://dx.doi.org/10.1007/s00211-013-0583-z
10. Hansbo, P.: Nitsche's method for interface problems in computational mechanics. GAMM-Mitt. 28(2), 183–206 (2005)
11. Lesinigo, M., D'Angelo, C., Quarteroni, A.: A multiscale darcy-brinkman model for fluid flow in fractured porous media. Numerische Mathematik 117(4), 717–752 (2011)
12. Pitkäranta, J.: Boundary subspaces for the finite element method with Lagrange multipliers. Numer. Math. 33(3), 273–289 (1979), http://dx.doi.org/10.1007/BF01398644
13. Saffman, P.: On the boundary condition at the surface of a porous media. Stud. Appl. Math. 50, 93–101 (1971)
14. Showalter, R.E.: Poroelastic filtration coupled to Stokes flow. In: Control theory of partial differential equations, Lect. Notes Pure Appl. Math., vol. 242, pp. 229–241. Chapman & Hall/CRC, Boca Raton, FL (2005), http://dx.doi.org/10.1201/9781420028317.ch16